ACS APPLIED MATERIALS & INTERFACES

Research Article

www.acsami.org

Printable Polymer Actuators from Ionic Liquid, Soluble Polyimide, and Ubiquitous Carbon Materials

Satoru Imaizumi, Yuto Ohtsuki, Tomohiro Yasuda, Hisashi Kokubo, and Masayoshi Watanabe*

Department of Chemistry and Biotechnology, Yokohama National University, 79-5 Tokiwadai, Hodogaya-ku, Yokohama 240-8501, Japan

Supporting Information

ABSTRACT: We present here printable high-performance polymer actuators comprising ionic liquid (IL), soluble polyimide, and ubiquitous carbon materials. Polymer electrolytes with high ionic conductivity and reliable mechanical strength are required for high-performance polymer actuators. The developed polymer electrolytes comprised a soluble sulfonated polyimide (SPI) and IL, 1-ethyl-3-methylimidazolium bis(trifluoromethanesulfonyl)amide ($[C_2mim][NTf_2]$), and they exhibited acceptable ionic conductivity up to 1×10^{-3} S cm^{-1} and favorable mechanical properties (elastic modulus $>1 \times 10^7$ Pa). Polymer actuators based on SPI/$[C_2mim][NTf_2]$ electrolytes were prepared using inexpensive activated carbon (AC) together with highly electron-conducting carbon such as acetylene black (AB), vapor grown carbon fiber (VGCF), and Ketjen black (KB). The resulting polymer actuators have a trilaminar electric double-layer capacitor structure, consisting of a polymer electrolyte layer sandwiched between carbon electrode layers. Displacement, response speed, and durability of the actuators depended on the combination of carbons. Especially the actuators with mixed AC/KB carbon electrodes exhibited relatively large displacement and high-speed response, and they kept 80% of the initial displacement even after more than 5000 cycles. The generated force of the actuators correlated with the elastic modulus of SPI/$[C_2mim][NTf_2]$ electrolytes. The displacement of the actuators was proportional to the accumulated electric charge in the electrodes, regardless of carbon materials, and agreed well with the previously proposed displacement model.

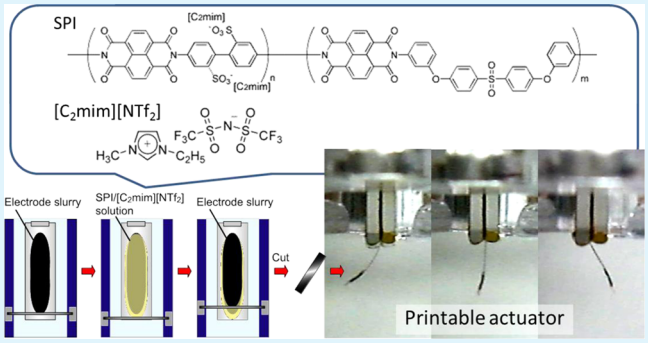

KEYWORDS: *polymer actuator, ionic liquid, sulfonated polyimide, polymer electrolyte, electric double layer capacitor*

INTRODUCTION

Polymer actuators have attracted much attention as next-generation driving parts because of properties such as their soft motion, flexibility, simple structure, and lightweight. In particular, electroactive polymer (EAP) actuators have high performance and a wide range of utility,[1] because they can be driven by easily controllable voltage application. EAP actuators are categorized into electronic and ionic EAP actuators. Ionic polymer−metal composite actuators,[2] conductive polymer actuators,[3] and carbon nanotube (CNT) actuators[4] have been proposed as ionic EAP actuators, and they are capable of large deformation even upon low voltage applications. However, their common drawback is the low durability under dry conditions, because of the evaporation of solvents that are incorporated into the ionic EAP actuators to dissociate and transport ions and/or ionic groups on polymers. Moreover, narrow electrochemical windows of water and organic solvents may limit the applied voltage and decrease the performance. For these reasons, ionic liquids (ILs) have been utilized as electrolytes for ionic EAP actuators[5−8] because of their unique physicochemical properties such as negligible volatility, high electrochemical stability, and high ionic conductivity, even in the absence of molecular solvents.

Generally, IL-based ionic EAP actuators consist of three materials: IL, electrode, and polymer. There are many studies on the effect of IL and electrode material structures on the performance of ionic EAP actuators.[5−12] Regarding the electrode materials, ionic EAPs generally require highly electronically conductive and high-surface-area electrode materials in order to achieve large and rapid deformation. In this sense, nonelectrolytically plated noble metals,[6] bucky gels[7] (CNTs dispersed in ILs), and poly(3,4-ethylenedioxythiophene)[8] are typical electrode materials. Indeed, the actuators using these electrodes exhibited large and rapid deformation and were stable even after thousands of cycles. On the other hand, previous studies on IL-based ionic EAP actuators have scarcely focused on polymeric materials. The transduction from electric energy into mechanical energy (generative force and displacement) should correlate closely with the properties of

Received: April 13, 2013
Accepted: June 5, 2013
Published: June 5, 2013

   dx.doi.org/10.1021/am401351q | ACS Appl. Mater. Interfaces 2013, 5, 6307−6315

Scheme 1. Synthesis of im-SPIs Having [C_2mim] Counter Cation

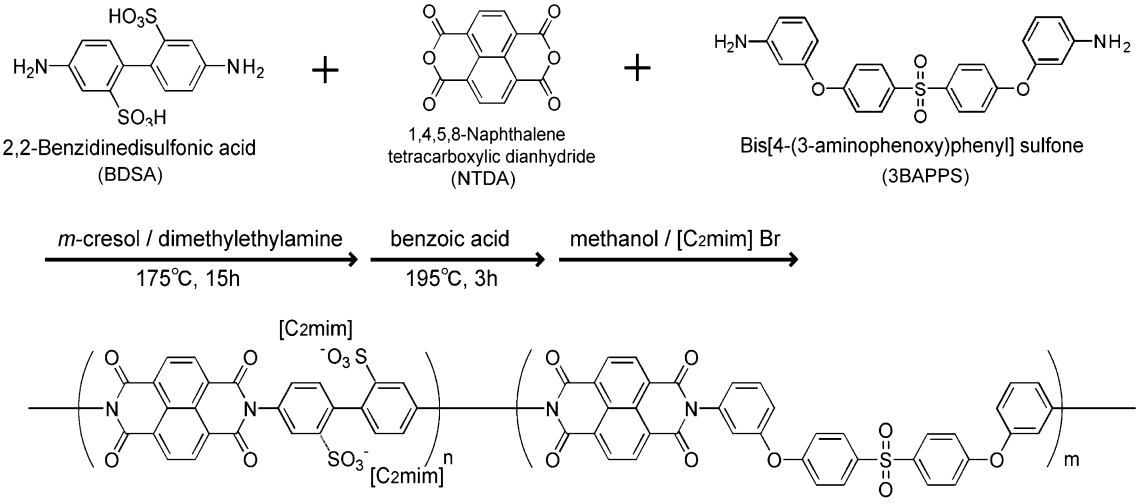

polymeric materials.[9] Optimization of polymeric materials forming the actuators is crucial and may bring about further improvement of performance. Commercially available poly(vinylidene fluoride-*co*-hexafluoropropylene) (P(VDF-*co*-HFP)) and Nafion have widely been used for IL-based ionic EAPs since they have good electrochemical and mechanical properties.[6,7,9−12] However, the exploration of suitable polymers for the actuators in terms of performance, processability, and durability is rather limited. Additionally, such investigations may also contribute to the progress in the fundamental understanding of transduction mechanisms. Very recently, for these reasons, studies on the polymeric materials for polymer actuators using IL are reported.[13,14] For instance, Long and co-workers prepared block copolymers for IL-containing EAP actuators.[13] Also, Hatipoglu et al. demonstrated applicability of sulfonated poly(arylene ether sulfone)s for the actuators.[14]

Polyimides are representative engineering plastics, which have high thermal stability, good film formability, and high mechanical strength. Studies on the application of polyimides to electrochemically functional materials have begun. In particular, sulfonated polyimides (SPIs) are expected to be alternative materials for Nafion as polymer electrolyte membranes of polymer electrolyte fuel cells (PEFCs).[15] Previously, we reported for the first time polymer electrolytes consisting of ILs and SPIs for nonhumidified PEFCs.[16] In SPI/IL electrolytes, rigid aromatic backbones of SPI make their films strong, and the sulfonate groups and their countercations provide compatibility with ILs. As a result, the polymer electrolytes of SPIs exhibit favorable mechanical properties in addition to high ionic conductivity.

We are interested in learning how polymeric materials can contribute to the high performance of IL-based EAP actuators. In particular, block copolymer self-assembly has been utilized to establish both highly conductive ion-conduction paths and reliable mechanical strength.[17] Furthermore, the applicability of ubiquitous and cheap carbon materials, such as carbon black and activated carbon, to IL-based EAP actuators has been demonstrated.[17] In this study, polymer electrolytes based on soluble SPI and IL, 1-ethyl-3-methylimidazolium bis(trifluoromethanesulfonyl)amide ([C_2mim][NTf_2]), were prepared to realize printable IL-based ionic EAP actuators with high performance and durability. The ionic EAP actuators were fabricated using these polymer electrolytes and carbon materials by printting method. Here, we discuss (1) the relationship between the electrolyte properties and the displacement and generated force responses of the actuators and (2) the effects of highly electron-conducting carbons added to activated carbon (AC) on the performance and durability of the actuators. The conducting carbons include acetylene black (AB), vapor-grown carbon fiber (VGCF), and Ketjen black (KB). We also rationalize the displacement response by using our previously proposed displacement model.[17b]

EXPERIMENTAL SECTION

Materials. 1,4,5,8-Naphthalene-tetracarboxylicdianhydride (NTDA, Aldrich) was washed by stirring in dimethylformamide (DMF) at 60 °C for 12 h, followed by rinsing by acetone. 2,2-Benzidinedisulfonic acid (BDSA) (Tokyo Chemical Industry) was purified by reprecipitation from water/triethylamine solution by adding aqueous 1 M H_2SO_4. Bis[4-(3-aminophenoxy)phenyl]sulfone (3BAPPS) (Wako Chemical) was recrystallized from ethanol. NTDA, BDSA, and 3BAPPS were dried in a vacuum oven at 80 °C prior to use. *m*-Cresol (Kanto Chemical) was dried using molecular sieves prior to use. *N*,*N*-Dimethylethylamine (Tokyo Chemical Industry) and benzoic acid (Junsei Chemical) were used without further purification. 1-Ethyl-3-methylimidazolium bromide ([C_2mim]Br) and [C_2mim][NTf_2] were synthesized according to a literature procedure[18] with slight modification. The water content in [C_2mim][NTf_2] determined by Karl Fischer titration was less than 10 ppm. AC, AB, VGCF, and KB were kindly provided by Kuraray, Denki Kagaku Kogyo, Showa Denko, and Lion, respectively.

Synthesis of SPI. SPIs having [C_2mim] countercation (im-SPI) were prepared by ion exchange reaction of SPIs with *N*,*N*-dimethylethylammonium (am-SPI) cation, according to the literature procedure[16a] shown in Scheme 1.

Polymerization of SPI was conducted by a procedure similar to that presented in our previous report.[16] The typical procedure is described as follows. BDSA (2.40 g, 6.96 mmol), 3BAPPS (0.75 g, 1.74 mmol), *N*,*N*-dimethylethylamine (1.27 g, 17.4 mmol), and 22 mL of *m*-cresol were added into a three-necked round-bottom flask, and this was followed by N_2 purge. The contents were stirred by a mechanical stirrer at 130 °C to dissolve the monomers, and then, NTDA (2.33 g, 8.7 mmol) was added. After stirring for 15 h at 175 °C, benzoic acid (2.5 g, 20 mmol) was added and the solution was stirred at 195 °C for another 3 h to complete the cyclodehydration. The reaction solution was cooled to 100 °C and diluted using 100 mL of *m*-cresol. Polymerized product was precipitated by dropping the solution into excess amount of acetone. The resulting fibrous precipitate was

washed by stirring in acetone overnight and then dried under vacuum at 60 °C for 24 h. Molecular weights and polydispersity indices were determined by gel permeation chromatography using a Shimadzu HPLC system (eluent: DMF with 0.01 M LiBr, column: Shodex LF-804 × 2 calibrated by polystyrene standards). The ion exchange capacity (IEC) was determined by titration. Properties of the resultant am-SPIs are summarized in Table 1. Am-SPI films, which were

Table 1. Molecular Weight, Polydispersity Index, and IEC of am-SPIs

	M_n	M_w	M_w/M_n	IEC (meq g^{-1})
am-SPI-1.52	1.47×10^5	4.86×10^5	3.30	1.52
am-SPI-2.37	1.79×10^5	5.42×10^5	3.02	2.37

prepared on a Petri dish by casting of *m*-cresol solution and evaporating the solvent on a hot plate at 60 °C for 48 h, were immersed in a methanol solution of $[C_2mim]Br$ and stirred for 72 h. The obtained films were washed with methanol and dried under vacuum at 60 °C. The $[C_2mim]$ cation exchange ratio of im-SPI was greater than 98%, as determined by ^1H NMR (AL-400 NMR spectrometer, JEOL).

Preparation and characterization of SPI/$[C_2mim][NTf_2]$. The im-SPI and $[C_2mim][NTf_2]$ were dissolved in *m*-cresol and stirred for 1 day. The mixture was cast on a Petri dish and dried on a hot plate at 60 °C for 48 h, followed by vacuum drying at 60 °C for 24 h. The films were vacuum-dried again at 60 °C for more than 5 h before use. Yellowish transparent free-standing films with $[C_2mim][NTf_2]$ contents of up to 75 wt % were successfully prepared without leaking of the $[C_2mim][NTf_2]$. A photograph of a SPI/$[C_2mim][NTf_2]$ film is shown in the Supporting Information, Figure S1. Differential scanning calorimetry (DSC) measurements were carried out on a DSC220C (SII NanoTechnology) under nitrogen atmosphere. The samples were sealed into Al pans under argon atmosphere, heated to 150 °C, cooled to −150 °C, and then, heated again to 150 °C at a rate of 10 °C min^{-1}. The DSC thermograms were recorded on the second heating scan. Ionic conductivity was evaluated by a complex impedance method utilizing a Hewlett-Packard 4192A LF impedance analyzer over a frequency range from 5 Hz to 13 MHz at an oscillation voltage of 10 mV. A circular film with a diameter of 11.5 mm was sandwiched between two stainless steel disk electrodes and encapsulated in a sealed cell in an Ar-filled glovebox (VAC, dew point < −80 °C). Conductivity measurements were carried out over a temperature range from 100 to −10 °C. The cell was stored for 1 h before taking measurements at each temperature. Dynamic viscoelastic measurements were conducted using film samples with a width of 5 mm and length of 20 mm, by DMS 210 (SII NanoTechnology) at a frequency of 1 Hz and a heating rate of 2 °C min^{-1}.

Preparation of Actuator. The actuators have a bimorph structure, and they were prepared by layer-by-layer printing. In this study, the precursor inks of the electrode and the electrolyte were prepared using only im-SPI-2.37. A *m*-cresol solution of SPI (5 wt %) and binary carbon powder, which consisted of 62 wt % of AC and 38 wt % of conducting additive such as AB, VGCF, or KB, were mixed in a mortar for 30 min. Then, $[C_2mim][NTf_2]$ was added and mixed for another 20 min. The obtained slurry contained SPI (10 wt %), binary carbon materials (30 wt %), and $[C_2mim][NTf_2]$ (60 wt %), excluding *m*-cresol. The slurry was coated by an automatic applicator (RK Print Coat Instruments Ltd., UK) onto an aluminum foil and dried for 24 h at 60 °C. The *m*-Cresol solution of SPI and $[C_2mim][NTf_2]$ was coated twice on a carbon electrode and dried at 60 °C. Finally, carbon slurry was coated again onto the electrolyte layer in the same way. The resultant trilaminar sheet was cut into 2 × 7 mm pieces, and the sample strips were peeled off from the aluminum foil.

Evaluation of Actuation. The actuator element was sandwiched between two 2-mm stainless steel foils attached on glass plates as a current corrector and fixed on one end. The current correctors were connected to an HA-301 potentiostat and an HB-104 function generator (Hokuto Denko). Displacement of the actuator was measured by a LC-2400 laser displacement meter (KEYENCE) at 4 mm from the clamped end. The voltage, current, and displacement were recorded on a PC using an NR-150 (KEYENCE) A/D converter. In this study, an average of half values of peak-to-peak positions was defined as a displacement value. Generative force measurement was carried out by using a load cell UL-2GR (Minebea) and a TA-802 generative force indicator (Sohgoh Keiso). An illustration of the experimental setup is shown in Figure 1.

Constant current charge−discharge measurements were conducted at 0 to ±500 mV vs Ag (quasi-reference electrode) with a current density of 200 mA per 1 g of AC using a three-electrode cell (a cross-sectional drawing of the cell is available in the Supporting Information, Figure S2) and a computer-controlled multipotentiostat (VMP2, Princeton Applied Research). Im-SPI-2.37/$[C_2mim][NTf_2]$ (SPI 25 wt %) electrolyte was sandwiched between two composite carbon electrodes (working and counter electrodes), which were prepared separately by the procedure above. Rest potential of the working electrode was close to 0 V. The long-term durability tests were carried out by applying ±1.5 V triangular waveform voltage at a scan rate of 500 mV s^{-1} (0.083 Hz).

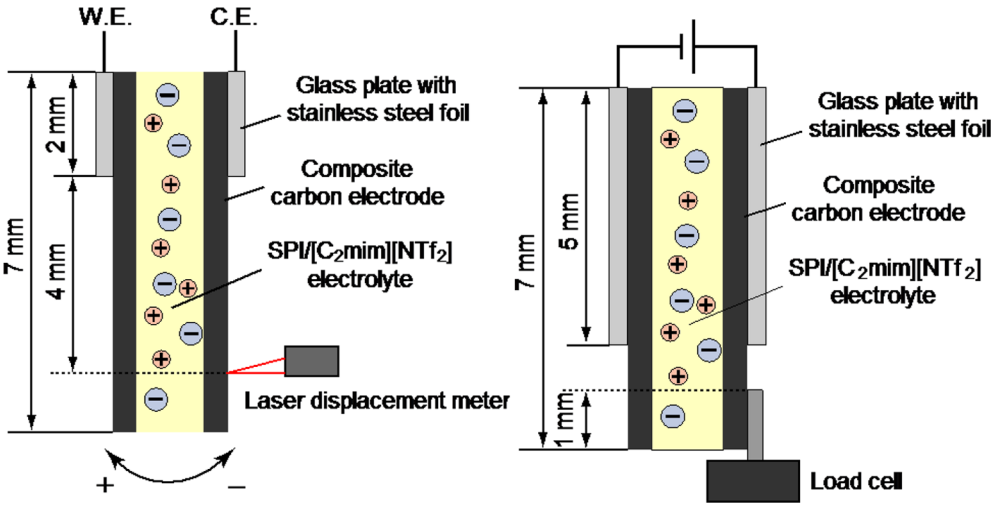

Figure 1. Experimental setup for the evaluation of displacement (left) and generative force (right) of the actuators.

RESULTS AND DISCUSSION

Characterization of SPI/[C_2mim][NTf_2] Electrolytes. DSC curves of im-SPI-2.37/[C_2mim][NTf_2] with different SPI fractions are shown in Figure 2. Although pure [C_2mim][NTf_2] exhibits exothermic and endothermic peaks assigned to crystallization (−49 °C) and melting (−18 °C) points, respectively, there are no peaks for the SPI/[C_2mim][NTf_2] with SPI fractions higher than 25 wt %. Similar to the previously reported SPI/protic ionic liquid[16] and poly(methyl methacrylate) (PMMA)/[C_2mim][NTf_2][19] systems, the crystallization of IL is prohibited by the interaction with im-SPI-2.37 polymer network. Hence, im-SPI can compatibly retain [C_2mim][NTf_2] in the polymer electrolyte up to 75 wt % without crystallization. It should be noted that a melting peak of [C_2mim][NTf_2] was observed in the case of im-SPI-1.52/[C_2mim][NTf_2] when the content of SPI was lower than 40 wt %, as shown in Figure S3 in the Supporting Information. This result suggests that the compatibility of SPI with [C_2mim][NTf_2] strongly depends on the IEC of SPI.

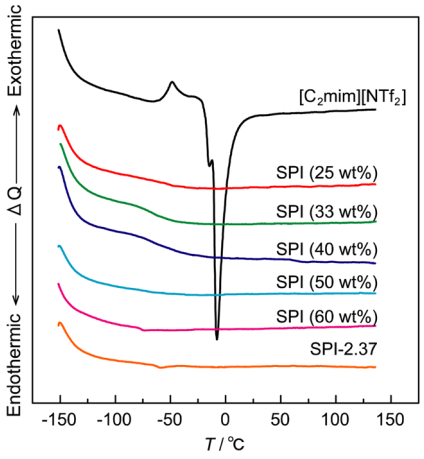

Figure 2. DSC thermograms for im-SPI-2.37/[C_2mim][NTf_2] with different SPI weight fractions.

Figure 3 shows the Arrhenius plots of the ionic conductivities of im-SPI-2.37/[C_2mim][NTf_2] and pure [C_2mim][NTf_2].[19] The ionic conductivities increase with decreasing SPI weight fractions and reach ca. 1 mS cm^{-1} at 20 °C for 25 wt % of SPI. It should be noted that the ionic conductivity of im-SPI-2.37/[C_2mim][NTf_2] was lower than that of im-SPI-1.52/[C_2mim][NTf_2] at the SPI composition of 33 wt % (see the Supporting Information, Figure S4). This result indicates that the compatibility between SPI and [C_2mim][NTf_2] greatly affects their ionic conductivity, and in this case, the leakage of [C_2mim][NTf_2] may contribute to the high ionic conductivity of im-SPI-1.52-based electrolytes. The leakage of IL from the electrolyte may cause the performance degradation, and therefore, the im-SPI-1.52-based electrolytes are not appropriate for the actuators in spite of their high ionic conductivity. While the ionic conductivity of SPI/[C_2mim][NTf_2] is relatively lower than that of pure [C_2mim][NTf_2], the ionic conductivity of im-SPI-2.37/[C_2mim][NTf_2] (SPI = 25 wt %) remained at ca. 0.1 mS cm^{-1} even at −10 °C. This result suggests that SPI/[C_2mim][NTf_2] electrolytes have enough ionic conductivity over a wide temperature range to be appropriate as electrolytes for electrochemical polymer actuators.

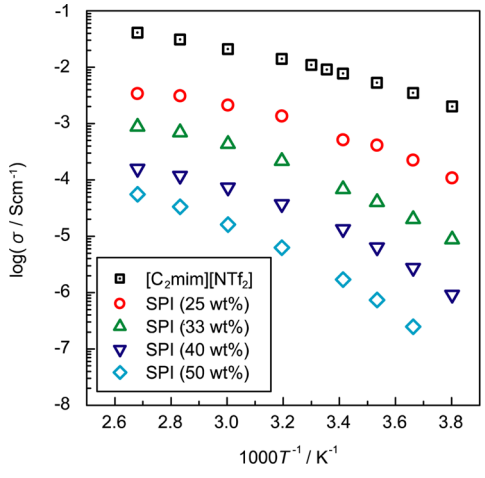

Figure 3. Temperature dependence of ionic conductivities for im-SPI-2.37/[C_2mim][NTf_2] electrolytes with different SPI content.

Table 2 summarizes the ionic conductivity (20 °C) and storage tensile modulus E' for different weight fractions of im-SPI-2.37/[C_2mim][NTf_2] and for related polymer electrolytes, determined by dynamic viscoelastic measurements at 30 °C. SPI/[C_2mim][NTf_2] electrolytes have high ionic conductivity comparable to the ion gel prepared of chemically cross-linked PMMA (0.98 mS cm^{-1} at 20 °C),[19] whereas the electrolytes have an elastic modulus that is more than 2 orders of magnitude higher. The P(VDF-*co*-HFP)-based electrolyte has high conductivity as well as high modulus, which is however caused by microporous structure generated by the phase separation of spherulites during the film-forming process.[20] [C_2mim][NTf_2] appears to be incorporated mainly into the porous structure, which causes the leakage of ionic liquid in a long-term use of the actuator.

Table 2. Ionic Conductivity and Storage Modulus for Different Polymer/[C_2mim][NTf_2] Electrolytes

polymer	$f_{polymer}$ (wt %)[a]	σ (mS cm^{-1})[b]	E' (MPa)[c]
im-SPI-2.37	25	0.83	37
im-SPI-2.37	33	0.29	220
im-SPI-2.37	50	0.0017	1100
im-SPI-2.37	100		6300
P(VDF-*co*-HFP)[d]	17	3.5	1.4
PMMA[e19]	21[d]	0.98	0.16

[a]Polymer weight percent in [C_2mim][NTf_2]-based electrolytes. [b]Ionic conductivity measured at 20 °C. [c]Storage tensile modulus measured at 30 °C. [d]Prepared by dissolving P(VDF-*co*-HFP) in [C_2mim][NTf_2] at 130 °C, followed by cooling to room temperature. [e]Network polymer cross-linked by ethylene glycol dimethacrylate (1 mol % vs MMA monomer).

Tensile moduli of the SPI-based electrolytes depend strongly on the SPI weight percent, and they have a range of approximately 2 orders of magnitude. The SPI-based electrolytes have 1×10^1−1×10^2 times higher tensile moduli than other polymer electrolytes with similar polymer weight fractions. Such exceptionally high tensile moduli of the SPI-based electrolytes are assumed to result from their rigid polymer backbone and microscopic structure. Temperature dependence of the viscoelastic properties of im-SPI-2.37/[C_2mim][NTf_2] is shown in Figure 4. There are two main

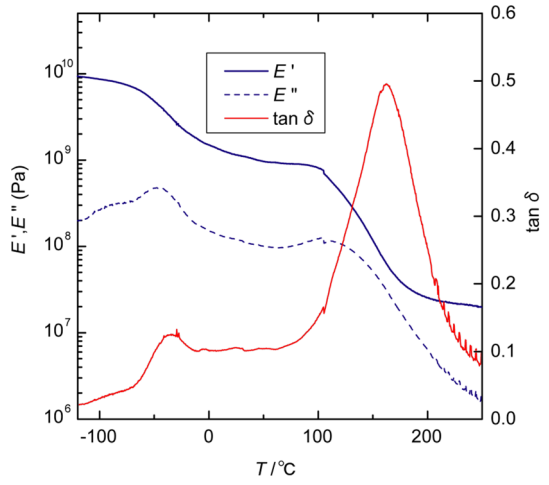

Figure 4. Storage tensile modulus (E'), loss modulus (E''), and loss tangent (tan δ) for SPI/[C_2mim][NTf_2] containing 50 wt % of im-SPI-2.37 measured at frequency of 1 Hz and scan rate of 2 °C min^{-1}.

relaxations in the storage tensile modulus: one is below 0 °C and the other is at temperatures higher than 100 °C. Both low and high relaxation temperatures decreased with increasing ionic liquid weight fractions. In the SPI/IL electrolyte, the hydrophobic and ionic groups appear to be phase-separated and the ionic liquid is preferentially incorporated in the ionic domains. The clustered ionic groups form ion-conducting channels, whereas the hydrophobic groups work as a rigid framework. As a result, SPI/IL electrolytes have microphase-separated structures; this is also supported by a tapping-mode AFM phase image of SPI/[C_2mim][NTf_2] (see the Supporting Information, Figure S5). Additional investigations are needed for detailed discussion about the morphology of SPI/[C_2mim]-[NTf_2]. Such an assumption coincides well with percolation-type changes in the ionic conductivity and elastic modulus of the SPI/IL electrolytes, as shown in this study and also in our previous work.[16] It has also been reported that SPIs prepared to replace perfluorinated sulfonic acid membranes in fuel cell applications have similar microphase-separated structures.[21,22]

Preparation and response of SPI/[C_2mim][NTf_2] actuators. Trilaminar-structured SPI/[C_2mim][NTf_2]-based actuators were successfully prepared by a layer-by-layer printing method, as described in the Experimental Section (see also the Table of Contents of this manuscript). Figure 5 shows an SEM image of the cross-sectional view of the actuator composed of

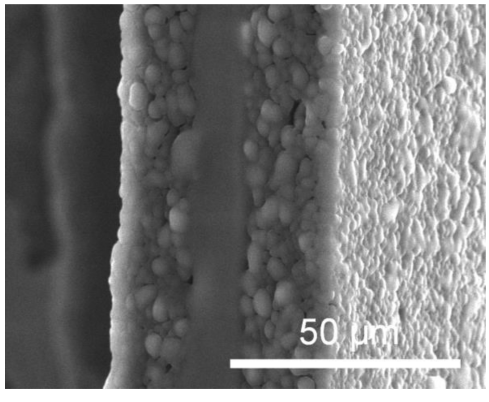

Figure 5. SEM image of cross-sectional view of an SPI actuator.

three distinct layers with total thickness of ca. 50 μm. In this image, the smooth inner layer is the SPI/[C_2mim][NTf_2] electrolyte (thickness of ca. 10 μm) and the rough outer layers are AB/AC/SPI/[C_2mim][NTf_2] composite electrodes (thickness of ca. 20 μm). It is difficult to peel off the electrodes from the electrolyte, because they adhere strongly. Accordingly, these layers are electrically well connected with each other, and facile ionic transport across the interlayer should be achieved.

By applying a ±1.5 V square waveform voltage at a frequency of 0.05 Hz, we investigated the displacement responses of the actuators, as shown in Figure 6: positive displacement indicates

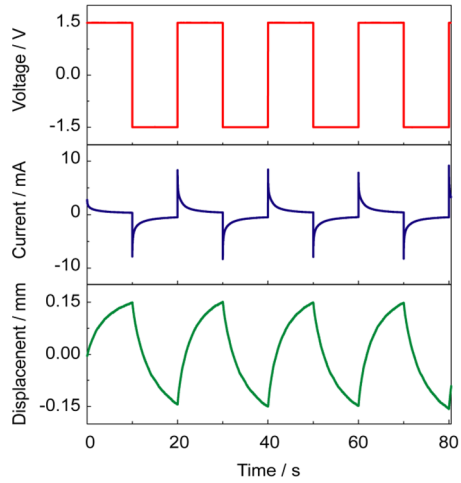

Figure 6. Response of an SPI actuator composed of AB/AC/SPI/[C_2mim][NTf_2] composite electrodes and SPI/[C_2mim][NTf_2] (SPI 25 wt %) electrolyte driven by a square waveform voltage of ±1.5 V at a frequency of 0.05 Hz.

bending toward the working electrode (W.E.) side (see Figure 1). The current response appears to be the charging current of electric double layer (EDL) at the interface between the carbon electrode and SPI/[C_2mim][NTf_2] in the electrode layer of the actuators, as we reported previously.[17] Cyclic voltammograms of the actuators (see the Supporting Information, Figure S6) were also typical for capacitors and did not exhibit Faradaic responses. However, the current decay in Figure 6 does not agree with a simple exponential function, as expected for an equivalent circuit with series combination of resistance and capacitance, due to relatively high longitudinal resistance of the carbon electrodes (vide infra). The actuators always bend toward the anodic side, and the absolute magnitude of the displacement increases with charging.

Figure 7 shows the maximum generative force of actuators at each applied voltage. The maximum force depends on the applied voltage and SPI composition in the electrolyte layer and increases with applied voltage and SPI fraction. Specifically, the actuator with an electrolyte containing 50 wt % of SPI generates a force of 68 mgf (stress of 67 MPa) at 3.0 V, and this composition reaches a force 70 times higher than its weight (ca. 1 mg), which is comparable to other IL-based actuators.[6,7,9] The SPI weight fraction dependence of generative force corresponds well to the difference in the elastic modulus of the electrolytes, as listed in Table 2.

Effect of Electron-Conducting Carbon Additives on Actuator Response. Figure 8 shows the displacement of the actuators (electrolyte layer contains 25 wt % of im-SPI-2.37) using three distinct electrodes, which contain different electron-

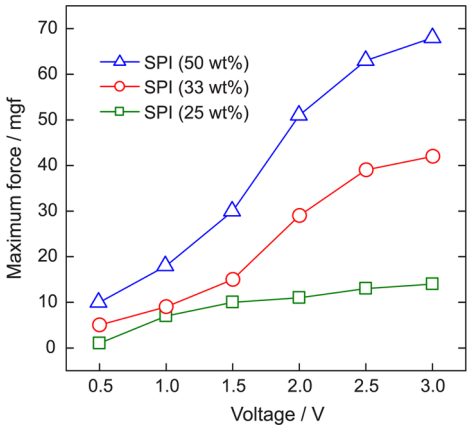

Figure 7. Maximum generative force of actuators using electrolytes with different SPI weight fractions as a function of voltage.

conducting carbon additives, as a function of voltage (Figure 8a) and as a function of accumulated charge (Figure 8b). In our previous study,[17b] it was demonstrated that displacement is proportional to the charge stored at EDL and is approximated by

$$\delta = \frac{L^2 Q}{3hqV_0}(t_+\nu_+ - t_-\nu_-) \quad (1)$$

,where δ is the displacement, L is the length from the fixed end to the laser-irradiating point, Q is the accumulated charge, h is the thickness, q is the elemental charge, V_0 is the initial volume of the electrode, t_+ is the cationic transference number, ν_+ is the cationic volume, t_- is the anionic transference number, and ν_- is the anionic volume. Figure 9 shows a dimensional drawing of our experimental setup for the displacement measurements. The solid line in Figure 8b was calculated using eq 1 and the parameters were as follows: L = 4 mm, h = 30 μm, q = 1.6 × 10^{-19} C, V_0 = 0.28 mm^3, t_+ = 0.63, ν_+ = 116 Å^3, t_- = 0.37, and ν_- = 147 Å^3. The value of h in eq 1 is not equal to the actual thickness (40 μm) of actuators, because there is a considerable difference in the strain between the inner face and the outer face of the electrode, since the electrode is not thin enough relative to the whole actuator. The efficient h was approximately h_e + h_i (30 μm), where h_e and h_i are the thicknesses of the electrodes and electrolyte, respectively (detailed explanation is given in Supporting Information).

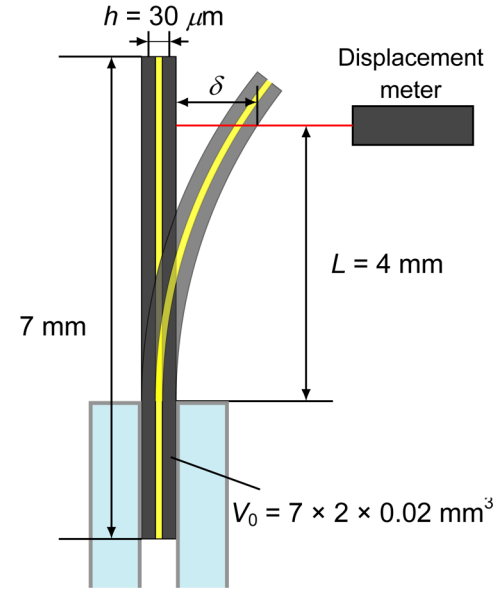

Figure 9. Dimensional drawing of the actuator.

A comparison among these three actuators with different electron-conducting additives reveals that VGCF- and AB-based actuators show similar magnitude of the displacement, as shown in Figure 8a. On the other hand, the displacement of KB-based actuator is 3−5 times larger. Figure 8b shows the correlation between the displacement δ and accumulated charge Q. Although the displacement response as a function of the magnitude of square wave voltage (Figure 8a) varies depending on the carbon materials, displacement δ can be represented by a single straight line when plotted against the accumulated charge Q. Furthermore, the experimental plots lie well on the calculated line. It should be noted that this relationship was observed when the applied voltage is lower than 4.0 V, which reflects the electrochemical potential window of the IL.[23] The linear relationship irrespective of selected carbon materials suggests that the driving mechanism of the actuator would be independent of the type of carbon. The large displacement of KB actuator in Figure 8a may be attributed to the large electric capacity of the composite electrode due to large specific surface area of KB (1270 m^2 g^{-1}). For more quantitative discussion, the EDL capacitances of composite

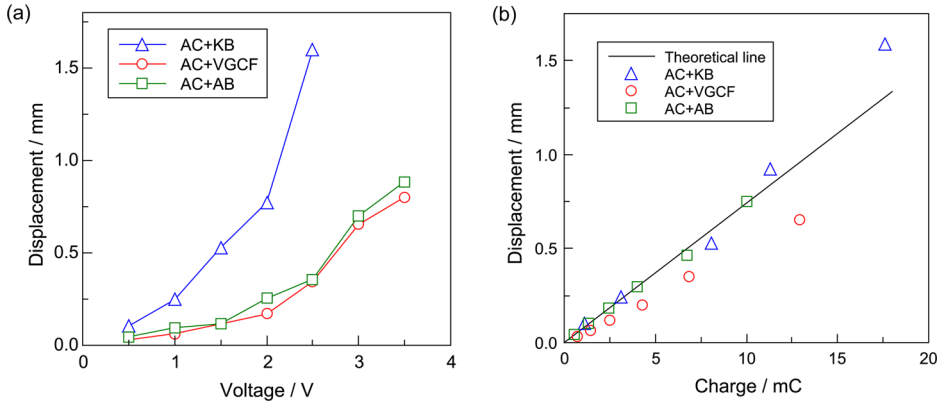

Figure 8. Maximum displacement of the actuators with different electron-conducting carbon additives in response to rectangular waveform voltages at a frequency of 0.05 Hz (a) as a function of applied voltage and (b) as a function of accumulated charge.

electrodes were measured by constant current charge−discharge measurements as follows.

EDL capacitances of the composite electrodes were measured using a three-electrode cell. Charge−discharge curves for the respective electrodes are shown in Figure 10, and

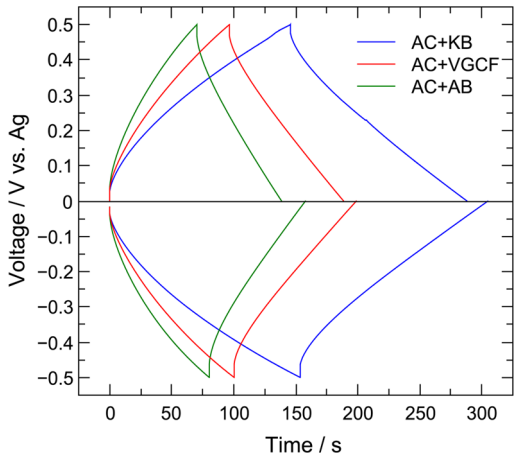

Figure 10. Charge−discharge curves of three different carbon electrodes measured by using a three-electrode cell.

cathodic and anodic capacitances (C_c and C_a, respectively) were determined separately by

$$C = \frac{I\Delta t}{w_{AC}\Delta V} \quad (2)$$

,where C is the electric double layer capacitance per AC weight, I is the current, $\Delta t/\Delta V$ is the slope of the discharge curve, and w_{AC} is AC weight in the working electrode. Table 3 summarizes

Table 3. Cathodic Capacitance (C_c) and Anodic Capacitance (C_a) of Carbon Electrodes

carbons	C_c (F g_{AC}^{-1})	C_a (F g_{AC}^{-1})
AC+AB	39	34
AC+VGCF	48	45
AC+KB	74	69

the EDL capacitances for these three electrodes. The cathodic capacitances are always higher than the anodic ones. This can be caused by higher affinity of $[C_2mim]$ cation with the carbon surface and by flatter and smaller shape of the cation compared with that of $[NTf_2]$ anion. Because of their affinity and shape, $[C_2mim]$ cations can closely exist at the vicinity of the carbon electrode surface and form thinner EDL. Based on the Helmholtz model, capacity is described by

$$C = \frac{\varepsilon_0\varepsilon_r}{d} \quad (3)$$

,where ε_0 is the vacuum permittivity, ε_r is the relative permittivity and d is the distance between the opposite charges in EDL. Equation 3 verifies that a small d induces a large C. The order of the magnitudes of capacities (both C_c and C_a) is AC +KB > AC+VGCF ≈ AC+AB, which is consistent with the order of the displacement magnitudes (Figure 8a). The difference in the EDL capacities depends on the difference in the characteristics of carbon additives, such as electronic conductivity and surface area, in comparison with those of AC. KB has not only high electronic conductivity but also large specific surface area, which contributes to the capacitance of the composite electrode, although the C_c and C_a values were calculated based on AC weight only.

The electron-conducting carbon materials affect not only the displacement magnitude but also the displacement speed. Figure 11 shows the scan rate dependence of the displacement

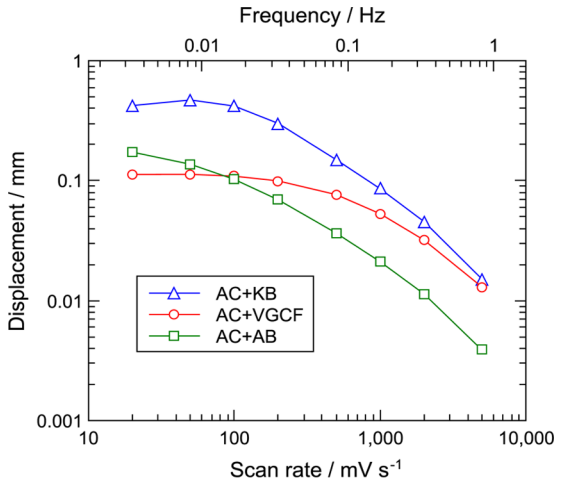

Figure 11. Scan rate dependence of the displacement of the actuators with different carbon electrodes driven by applying ±1.5 V triangular waveform voltage.

of the actuators with different carbon electrodes. In high-frequency range, the displacement magnitude dominantly correlates with the electronic conductivity of composite carbon electrodes. Actuators with KB- and VGCF-based electrodes exhibit larger displacement at the frequencies exceeding 0.1 Hz than the one based on AB, due to their high electronic conductivity (ca. 20 mS cm^{-1} vs ca. 10 mS cm^{-1} for the AB-based electrode). On the other hand, in low-frequency range, the displacement magnitude mainly correlates with capacitance. The KB-based actuator exhibits larger displacement than the others, as seen in Figure 8a. In general, the KB-based actuator exhibits superior performance over the whole frequency range, and we can conclude that KB is the most suitable conducting additive for the actuators, among the carbon materials used in this study.

Durability of Actuators. The durability of the actuators was estimated by continuous triangular voltage application experiments. Figure 12 shows the displacement change as a function of cycle number for the actuators with different carbon electrodes at an applied voltage of ±1.5 V and a scan rate of 0.5 V s^{-1} (0.083 Hz). The displacement gradually decreases with cycle number. However, the actuators exhibit displacement of at least 60% of the initial value even after 5000 cycles. Additionally, no faradaic reactions were observed at these experimental conditions, and there were no macroscopic damages in the structure of the actuators. Hence, the durability can be ascribed to the electrochemical stability of ionic liquid, favorable mechanical properties of SPI, and stable lamination of the electrodes and the electrolyte. Among the three carbon electrodes, the KB-based one exhibited the most stable behavior, and the displacement remained at 80% of the initial value after 5000 cycles. To identify the cause of the degradation for the actuators with AB and VGCF electrodes, we measured complex impedance spectroscopy before and after the cycle stability test, shown in the Supporting Information, Figure S7.

dx.doi.org/10.1021/am401351q | ACS Appl. Mater. Interfaces 2013, 5, 6307−6315

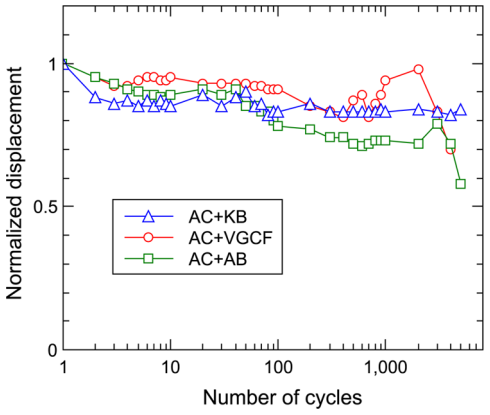

Figure 12. Normalized displacement of the actuators as a function of cycle number with the application of ±1.5 V triangular waveform voltage at a scan rate of 0.5 V s^{-1}.

A significant increase in the electrode resistance was observed for the actuators with AB electrodes. It is likely that this increase was caused by the loss of the connection between the carbon particles because of the repetitive strain of the electrode.

CONCLUSIONS

We have developed a polymer electrolyte based on SPI and IL ($[C_2mim][NTf_2]$), which exhibits high mechanical strength, thin film formability, and high ionic conductivity. Hence, it is suitable for electrochemical polymer actuators. By using a polymer electrolyte and ubiquitous carbon materials, polymer actuators with thicknesses of ca. 50 μm were successfully prepared by repeated printing. The actuators exhibited relatively large displacements and wide potential window of up to 3.5 V. Particularly noticeable improvement of the actuator in terms of displacement magnitude and response speed could be achieved by utilizing KB as an electron-conducting additive in the electrode layer. The displacement was proportional to the stored electric charge in the actuator element, and this result agreed with eq 1 regardless of the type of carbon material. The generative force of the actuators depended on the elastic modulus and reached values up to 70 times higher than their weight. The actuators also showed good durability of more than 5000 cycles, and KB-based actuator exhibited more stable behavior.

ASSOCIATED CONTENT

Supporting Information

Photograph of polymer electrolyte film (Figure S1), structure of three-electrode cell (Figure S2), DSC thermograms (Figure S3), ionic conductivities (Figure S4), AFM images (Figure S5), cyclic voltammograms (Figure S6), Nyquist plots (Figure S7), and the effective thickness deviation of actuator (Figures S7 and S8). This material is available free of charge via the Internet at http://pubs.acs.org.

AUTHOR INFORMATION

Corresponding Author

*E-mail: mwatanab@ynu.ac.jp. Tel and fax: +81-45-339-3955.

Notes

The authors declare no competing financial interest.

ACKNOWLEDGMENTS

This work was supported in part by Grants-in-aid for Scientific Research on Priority Areas (438-19016014 and 452-17073009) and Basic Research A (23245046) from the MEXT of Japan.

REFERENCES

(1) (a) *Application of Electroactive Polymers*; Scrosati, B., Ed.; Chapman & Hall: London, 1993. (b) *Electroactive Polymer (EAP) Actuators as Artificial Muscles*; Bar-Cohen, Y., Ed.; SPIE Press: Bellingham, WA, 2001.

(2) (a) Asaka, K.; Oguro, K.; Nishimura, Y.; Mizuhata, M.; Takenaka, H. *Polym. J.* **1995**, *27*, 436. (b) Shahinpoor, M. *Electrochim. Acta* **2003**, *48*, 2343.

(3) (a) Kaneto, K.; Kaneko, M.; Min, Y.; MacDiarmid, A. G. *Synth. Met.* **1995**, *71*, 2211. (b) Baughman, R. H. *Synth. Met.* **1996**, *78*, 339. (c) Smela, E. *Adv. Mater.* **2003**, *15*, 48.

(4) Baughman, R. H.; Cui, C.; Zakhidov, A. A.; Iqbal, Z.; Barisci, J. N.; Spinks, G. M.; Wallace, G. G.; Mazzoldi, A.; Rossi, D. D.; Rinzler, A. G.; Jaschinski, O.; Roth, S.; Kertesz, M. *Science* **1999**, *284*, 1340.

(5) Lu, W.; Fadeev, A. G.; Qi, E.; Smela, B. H.; Mattes, B. R.; Ding, J.; Spinks, G. M.; Mazurkiewicz, J.; Zhou, D. Z.; Wallace, G. G.; MacFarlane, D. R.; Forsyth, S. A.; Forsyth, M. *Science* **2002**, *297*, 983.

(6) (a) Bennett, M. D.; Leo, D. J. *Sens. Actuators A* **2004**, *115*, 79. (b) Akle, B. J.; Bennett, M. D.; Leo, D. J. *Sens. Actuators A* **2006**, *126*, 173.

(7) (a) Fukushima, T.; Asaka, K.; Kosaka, A.; Aida, T. *Angew. Chem., Int. Ed.* **2005**, *44*, 2410. (b) Mukai, K.; Asaka, K.; Kiyohara, K.; Sugino, T.; Takeuchi, I.; Fukushima, T.; Aida, T. *Electrochim. Acta* **2008**, *53*, 5555.

(8) Vidal, F.; Plesse, C.; Teyssié, D.; Chevrot, C. *Synth. Met.* **2004**, *142*, 287.

(9) Sugino, T.; Kiyohara, K.; Takeuchi, I.; Mukai, K.; Asaka, K. *Sens. Actuators B* **2009**, *141*, 179.

(10) (a) Takeuchi, I.; Asaka, K.; Kiyohara, K.; Sugino, T.; Terasawa, N.; Mukai, K.; Shiraishi, S. *Carbon* **2009**, *47*, 1373. (b) Takeuchi, I.; Asaka, K.; Kiyohara, K.; Sugino, T.; Terasawa, N.; Mukai, K.; Fukushima, T.; Aida, T. *Electrochim. Acta* **2009**, *54*, 1762. (c) Terasawa, N.; Takeuchi, I.; Matsumoto, H. *Sens. Actuators, B* **2009**, *139*, 624. (d) Terasawa, N.; Takeuchi, I.; Matsumoto, H.; Mukai, K.; Asaka, K. *Sens. Actuators B* **2011**, *156*, 539.

(11) Lee, J.-W.; Yoo, Y.-T. *Sens. Actuators B* **2009**, *137*, 539.

(12) (a) Palmre, V.; Brandell, D.; Mäeorg, U.; Torop, J.; Volobujeva, O.; Punning, A.; Johanson, U.; Kruusmaa, M.; Aabloo, A. *Smart Mater. Struct.* **2009**, *18*, 095028. (b) Torop, J.; Palmre, V.; Arulepp, M.; Sugino, T.; Asaka, K.; Aabloo, A. *Carbon* **2011**, *49*, 3113.

(13) (a) Gao, R.; Wang, D.; Heflin, J. R.; Long, T. E. *J. Mater. Chem.* **2012**, *22*, 13473. (b) Green, M. D.; Wang, D.; Hemp, S. T.; Choi, J.-H.; Winey, K. I.; Heflin, J. R.; Long, T. E. *Polymer* **2012**, *53*, 3677. (c) Wu, T.; Wang, D.; Zhang, M.; Heflin, J. R.; Moore, R. B.; Long, T. E. *ACS Appl. Mater. Interfaces* **2012**, *4*, 6552.

(14) Hatipoglu, G.; Liu, Y.; Zhao, R.; Yoonessi, M.; Tigelaar, D. M.; Tadigadapa, S.; Zhang, Q. M. *Smart Mater. Struct.* **2012**, *21*, 055015.

(15) Hickner, M. a; Ghassemi, H.; Kim, Y. S.; Einsla, B. R.; McGrath, J. E. *Chem. Rev.* **2004**, *104*, 4587.

(16) (a) Lee, S.-Y.; Ogawa, A.; Kanno, M.; Nakamoto, H.; Yasuda, T.; Watanabe, M. *J. Am. Chem. Soc.* **2010**, *132*, 9764. (b) Yasuda, T.; Nakamura, S.; Honda, Y.; Kinugawa, K.; Lee, S.-Y.; Watanabe, M. *ACS Appl. Mater. Interfaces* **2012**, *4*, 1783.

(17) (a) Imaizumi, S.; Kokubo, H.; Watanabe, M. *Macromolecules* **2012**, *45*, 401. (b) Imaizumi, S.; Kato, Y.; Kokubo, H.; Watanabe, M. *J. Phys. Chem. B* **2012**, *116*, 5080. (c) Saito, S.; Katoh, Y.; Kokubo, H.; Watanabe, M.; Maruo, S. *J. Micromech. Microeng.* **2009**, *19*, 035005.

(18) Tokuda, H.; Hayamizu, K.; Ishii, K.; Susan, M. A. B. H.; Watanabe, M. *J. Phys. Chem. B* **2005**, *109*, 6103.

(19) Susan, M. A. B. H.; Kaneko, T.; Noda, A.; Watanabe, M. *J. Am. Chem. Soc.* **2005**, *127*, 4976.

(20) Michot, T.; Nishimoto, A.; Watanabe, M. *Electrochim. Acta* **2000**, *45*, 1347.

(21) (a) Essafi, W.; Gebel, G.; Mercier, R. *Macromolecules* **2004**, *37*, 1431. (b) Gebel, G.; Diat, O. *Fuel Cells* **2005**, *5*, 261.
(22) Bae, B.; Yoda, T.; Miyatake, K.; Uchida, H.; Watanabe, M. *Angew. Chem., Int. Ed.* **2010**, *49*, 317.
(23) Bonhote, P.; Dias, A.-P.; Papageorgiou, N.; Kalyanasundaram, K.; Grätzel, M. *Inorg. Chem.* **1996**, *35*, 1168.